IEEE Access
Multidisciplinary | Rapid Review | Open Access Journal

Received May 14, 2021, accepted June 8, 2021, date of publication June 15, 2021, date of current version June 29, 2021.

*Digital Object Identifier 10.1109/ACCESS.2021.3089489*

# Double-Layer Ku/K Dual-Band Orthogonally Polarized High-Efficiency Transmitarray Antenna

**MINGBO CAI, ZEHONG YAN, FANGFANG FAN, (Member, IEEE), SHUYANG YANG, AND XI LI**

National Key Laboratory of Antenna and Microwave Technology, Xidian University, Xi'an 710071, China

Corresponding author: MingBo Cai (bluecb@126.com)

**ABSTRACT** This paper presents a double-layer, dual-band, orthogonally polarized, highly efficient transmitarray antenna (TA) operated in the Ku/K band (14 GHz/20 GHz) for millimeter wave (MMW) wireless communication systems (WCS). The proposed TA consists of two types of multi-resonant dipoles with metal vias, operating in the Ku and K bands. The Ku and K elements are interlaced with each other independently to ensure dual-band orthogonally polarized operation. The proposed double-layer elements obtained a 360° phase shift range with transmission amplitude greater than −2 dB. They also achieved independent phase responses in both bands by two orthogonally arranged elements. The proposed TA has been designed, manufactured and measured. The measurement results, which are consistent with simulation results, indicate that maximum gains of 25.2 and 27.4 dBi corresponding to aperture efficiencies of 55% and 49% are obtained at 13.75 and 20 GHz, respectively. Moreover, 1-dB gain bandwidths of 10% and 6% are also achieved in the Ku and K frequency bands, respectively. Therefore, the proposed double-layer Ku/K dual-band TA with high efficiency and simple design is a good candidate for MMW WCS.

**INDEX TERMS** Double-layer, dual-band, orthogonally polarized, transmitarray.

## I. INTRODUCTION

Planar antennas (e.g., transmitarray antennas (TAs) and reflectarray antennas (RAs)) have received extensive research attention because of their advantages of high gain, light weight, low cost and ease of fabrication using printed circuit board technology [1]–[24]. TAs inherited the merits of RAs and eliminated the feed blockage. Although TAs have many advantages, challenges still remain when designing high-performance TAs. When designing a TA, both amplitude and phase shift must be considered. However, in general, only the phase shift needs to be considered for the RA. Through years of research and development, various TA design methods have been proposed and developed [5]–[22].

In general, the relationship between the amplitude, phase shift range and layer are somewhat fixed according to the theoretical limit [4], [5]. Therefore, to achieve good transmission amplitude and sufficient phase shift range, a multi-layer stacked structure is typically used [6]–[10]. However, the multi-layer structure inevitably introduces inherent disadvantages, such as increased thickness, mass, cost and assembly error. Therefore, developing TAs with a double-layer structure has practical significance.

Some studies have designed TAs with a double-layer structure [11]–[19]. However, in previous research [11]–[14], the TA element with a double-layer structure could not realize 360° full transmission phase coverage without degenerating the amplitude [4], [5]. Metal vias have been introduced in past studies [15]–[19] to expand the phase shift range and improve the transmission amplitude of double-layer TAs. In particular, a 305° phase shift range was achieved using a double-layer structure with metal vias [15]. In other studies, a 360° phase shift range with an insertion loss of less than −2 dB was achieved [16]–[20]. However, the abovementioned double-layer TAs work in a single frequency band, and because the frequency spectrum is not fully utilized, the applications of these TAs are limited. Therefore, developing a dual-band TA using a double-layer structure is necessary.

Although numerous challenges remain in terms of designing dual-band TAs, some outstanding designs have been presented [21]–[25]. For example, a dual-band TA has been proposed using a four-layer structure, and a 360° phase shift range with transmission magnitude greater than −3 dB has been obtained in both bands [21]. Although it achieved high

The associate editor coordinating the review of this manuscript and approving it for publication was Tutku Karacolak.

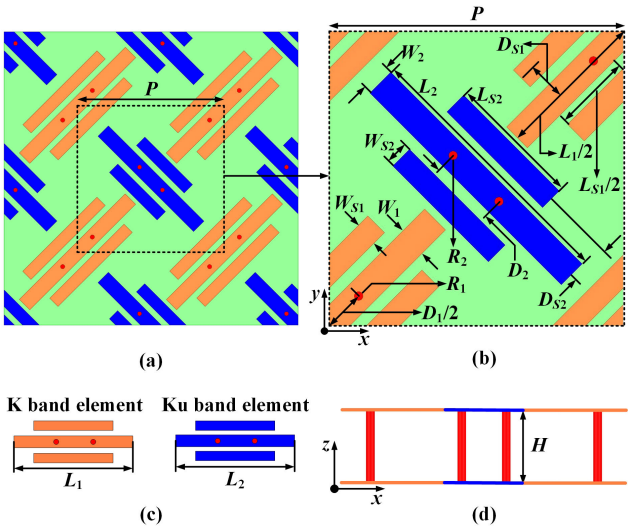


**FIGURE 1.** Configuration of the proposed element. (a) Element arrangement. (b) Top and bottom view of the periodic element. (c) Element diagram. (d) Side view.

aperture efficiencies of 52% and 53% at 12 and 18 GHz, respectively, it has a narrow bandwidth and high side-lobe levels in both bands. Another study [22] proposed a dual-band TA operating in the Ka band using a three-layer structure. The proposed unit-cell exhibited a 180° phase resolution in both bands and aperture efficiencies of ∼20% and 21% at 29 and 19.5 GHz, respectively. Another study [23] proposed a three-layer, dual-band, dual-polarized metallic slot TA, which achieved 1-dB gain bandwidths of 6.8% and 5.4% as well as aperture efficiencies of 38% and 34.6% at 11 and 12.5 GHz, respectively. A dual-band (12.25 GHz/14.25 GHz) orthogonally polarized TA was proposed in [24], wherein the TA element consists of a triple-dipole, three-layer configuration. This design achieved a 300° phase shift range and achieved aperture efficiencies of 45% and 41.3% and 1-dB gain bandwidths of 7.2% and 7.0% at 12.5 and 14.25 GHz, respectively. In [25], a dual-band and dual-polarized TA using a three-layer structure was presented in which the two types of loop elements are interlaced with each other and operate independently in two different bands (12.5 GHz/14.25 GHz). A 300° phase shift range with transmission amplitude greater than −2 dB is achieved in both bands. However, the above-mentioned dual-band TAs use a multi-layer stacked structure, and most of them operate at closely spaced frequencies, which leaves room for improvement.

Additionally, antennas polarized at ±45° are widely used in WCS and mobile base stations [26]–[28]. Developing a TA with ±45° polarization is significant, although related studies are still at the initial stage. In this letter, a double-layer, dual-band (14 GHz/20 GHz) orthogonally polarized highly efficient TA is presented. Details of the design process of the proposed TA are provided below. The remainder of this articles is organized as follows. Section II presents the dual-band element diagram and element performances.

**TABLE 1.** Dimensions of the corresponding variables.

| PARAMETER | VALUE | PARAMETER | VALUE |
|---|---|---|---|
| $P$ | 10MM | $H$ | 2 MM |
| $L_1$ | 5~10.2 MM | $L_2$ | 3~9.2 MM |
| $L_{S1}$ | $L_1$*$A_1$ | $L_{S2}$ | $L_2$* $A_3$ |
| $A_1$ | 0.7 | $A_3$ | 0.5 |
| $W_1$ | 1MM | $W_2$ | 1MM |
| $W_{S1}$ | 0.8MM | $W_{S2}$ | 0.8MM |
| $D_1$ | $L_1$* $A_2$ | $D_2$ | $L_1$* $A_4$ |
| $A_2$ | 0.14 | $A_4$ | 0.12 |
| $D_{S1}$ | 1.3 MM | $D_{S2}$ | 1.3 MM |
| $R_1$ | 0.15MM | $R_2$ | 0.15MM |

Section III presents the dual-band TA design and the simulated and measured results. This Section also presents the comparisons between the proposed TA and other existing dual-band TAs. Finally, the conclusions are presented in Section IV.

## II. DUAL-BAND ELEMENT DESIGN AND PERFORMANCES

### A. ELEMENT CONFIGURATION

The element of the proposed double-layer TA is operated with orthogonally linear polarization (LP), the Ku band element works at 45° LP, and the K band element works at −45° LP. To achieve a compromise between the two frequency bands, the element spacing is set at 10 mm ($P$ = 10 mm, which corresponds to 0.47λ at 14 GHz and 0.67λ at 20 GHz). The geometry of the proposed element is shown in Fig. 1. The proposed Ku and K band elements consist of two multi-resonant dipoles and two metal vias. The two types of elements are interlaced with each other independently to ensure a dual-band orthogonally polarized operation. Then, these are fabricated on both sides of the dielectric substrate with a relative permittivity of 2.2 and a loss tangent of 0.0009 ($\varepsilon_r$ = 2.2, $\tan\delta$ = 0.0009). The two metal vias connect the top and bottom dipoles. The detailed dimensions of the proposed element are shown in Table 1.

### B. ELEMENT PERFORMANCE

The proposed dual-band orthogonally polarized element is established and simulated in a high-frequency structure simulator (HFSS) based on the finite element method. The simulated transmission responses of the proposed element without metal vias are shown in Fig. 2. The two elements have magnitude skips and phase jumps at 14 and 20 GHz, respectively, thus resulting in poor transmission amplitude and limited phase shift range.

The simulated performances of the proposed elements with metal vias are shown in Fig. 3. As demonstrated in Fig. 3(a), a 360° phase shift range with transmission magnitude greater than −2 dB is obtained at 14 GHz when $L_1$ varies from 5–10.2 mm. Similarly, as shown in Fig. 3(b), when $L_2$ varies from 3–9.2 mm, a full phase shift range of 360° and a transmission magnitude greater than −2 dB is achieved also at 20 GHz.

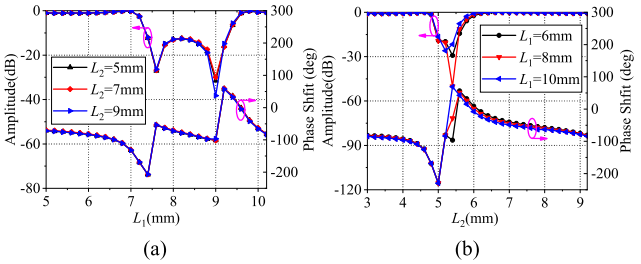


**FIGURE 2.** Transmission magnitude and phase shift of the proposed element without vias. (a) 14 GHz. (b) 20 GHz.

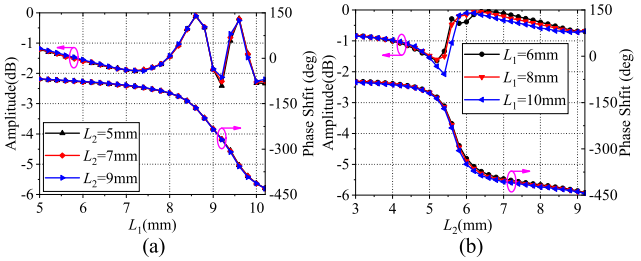


**FIGURE 3.** Transmission magnitude and phase shift of proposed element with vias. (a) 14 GHz. (b) 20 GHz.

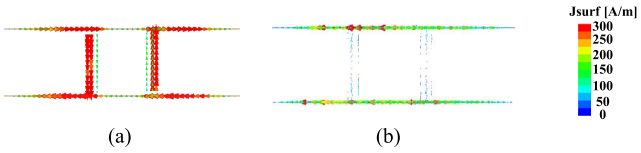


**FIGURE 4.** The current distribution of the Ku band element at different sizes. (a): $L_1 = 9$ mm, (b): $L_1 = 10$ mm.

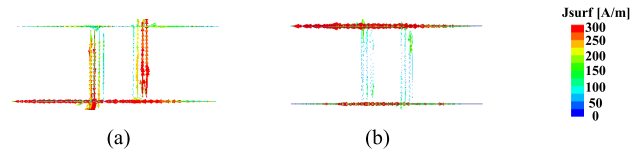


**FIGURE 5.** The current distribution of the K band element at different sizes. (a): $L_2 = 5.4$ mm, (b): $L_2 = 6.5$ mm.

The functions of the metal vias have been discussed in [15]. At 14 GHz, on the one hand, when $L_1$ varies from 7–9.5 mm, the metals vias transmit the energy from the upper dipoles to the lower dipoles due to the weak coupling between the upper and lower layers, and the element is working in a receive/transmit mode, as shown in Fig. 4(a). On the other hand, the vias have almost no effect on the element performances in the other range of $L_1$, as shown in Fig. 4(b). The element is working by coupling of the upper and lower dipoles. The same operating principle is adopted at 20 GHz. The vias is an indispensable part of the elements when $L_2$ varies from 4.8–6 mm, as demonstrated in the Fig. 5(a). However, the vias contribute little in other cases, as exhibited in the Fig. 5(b). The metal vias improve the transmission efficiency greatly and make it possible for a double-layer TA

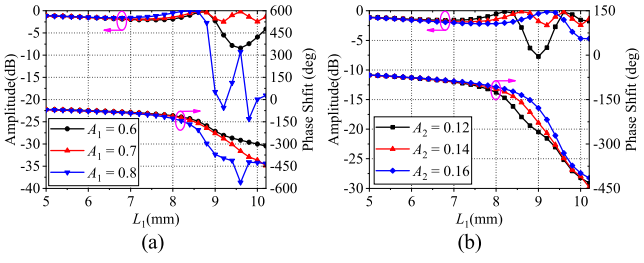


**FIGURE 6.** Transmission responses of proposed element with different parameters at 14 GHz. (a) Transmission responses with different parameters of $A_1$. (b). Transmission responses with different parameters of $A_2$.

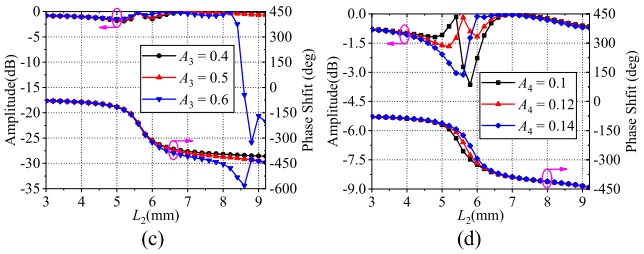


**FIGURE 7.** Transmission responses of proposed element with different parameters at 20 GHz. (a) Transmission responses with different parameters of $A_3$. (b). Transmission responses with different parameters of $A_4$.

to achieve a 360° phase shift range without attenuating the transmission magnitude.

Transmission amplitude and phase shift of proposed element with different parameters at 14 and 20 GHz are shown in Fig. 6 and Fig. 7, respectively. As demonstrated in Fig. 6(a), the transmission magnitude and phase shift of the proposed element vary with different values of $A_1$. The phase shift range is less than 260° with transmission magnitude greater than −8 dB when the $A_1 = 0.6$, and a full phase shift range of 360° with transmission magnitude greater than −2 dB is obtained when the $A_1$ increases to 0.7. However, magnitude skips and phase jumps are appeared when the $A_1 = 0.8$. In Fig. 6(b), considering both transmission magnitude and slope of phase shift curves, the $A_2$ is chosen as 0.14. The same working principle can also be seen from Figure 7 in K band. Finally, the optimal values of parameters are set as $A_1 = 0.7$, $A_2 = 0.14$, $A_3 = 0.5$ and $A_4 = 0.12$. The transmission magnitude and phase shift of proposed element in the band are also shown in Fig. 8.

### C. OBLIQUE INCIDENCE PERFORMANCE

The incident angles of the elements vary with the location of the unit. Therefore, the responses of the elements at different incident angles are the critical factors for a good TA design. In the proposed dual-band TA design, the maximum incident angle of the element is 20°, which is dependent on the edge illumination (EI) level of the feed horn for maximum efficiency [29]. The simulated results of the proposed element under different incident angles are shown in Fig. 9 to

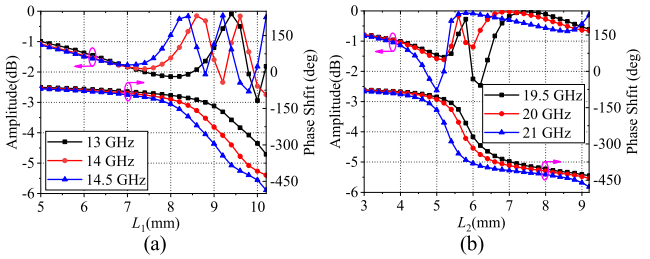


**FIGURE 8.** Transmission magnitude and phase shift of proposed element in the band. (a) Ku band. (b) K band.

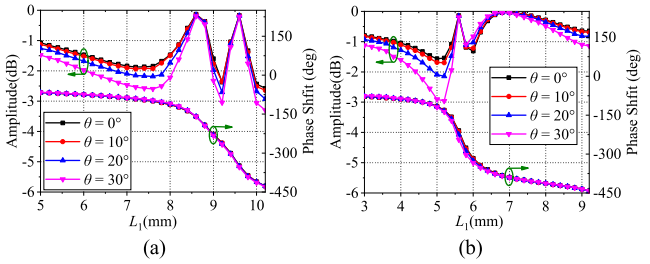


**FIGURE 9.** Transmission magnitudes and phase shifts of the proposed elements with different oblique incidences at 14 and 20 GHz. (a) 14 GHz, (b) 20 GHz.

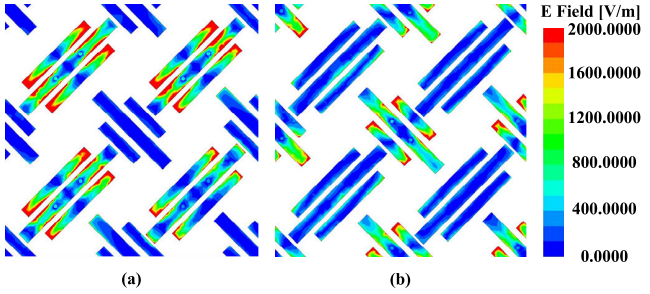


**FIGURE 10.** Surface current distributions of the dual-band TA at (a) 14 GHz and (b) 20 GHz.

evaluate the phase stability of the element. At 14 and 20 GHz, the proposed elements maintain good performances with different incident angles. Although minor variations appear in the transmission phase responses, especially at 20 GHz, these differences are acceptable in the TA design. In reality, the maximum phase differences of the proposed element in both bands are less than 30° within incident angles of 20°. Therefore, the phase responses of the elements under normal incidence at 14 and 20 GHz are used to design the proposed dual-band TA to simplify the design method.

### D. ELEMENT INDEPENDENCE

The Ku and K band elements are interlaced with each other independently to ensure a dual-band orthogonally polarized operation. The isolation between the two types of elements at 14 and 20 GHz is studied. The surface current distributions of the proposed TA are shown in Fig. 10. As seen in Fig. 10(a), at 14 GHz, the Ku band element has a strong current distribution but no distribution on the K band element. Similarly,

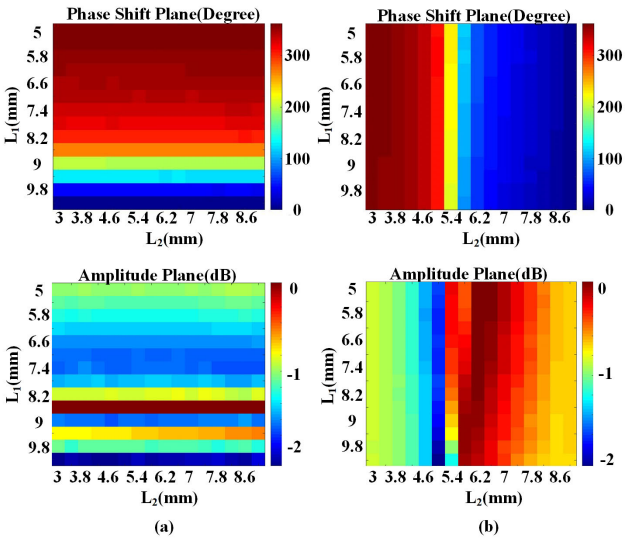


**FIGURE 11.** The transmission responses at (a) 14 GHz and (b) 20 GHz. (The phase responses are in the top row, and the amplitude responses are in the bottom row).

as indicated in Fig. 10(b), the surface current distributions are mostly focused on the K band element, and the Ku band element has little or no response at 20 GHz.

The independences between the Ku and K band elements are further analyzed, and all the possible combinations of parameters of $L_1$ and $L_2$ at both frequencies are shown in Fig. 11. As demonstrated in Fig. 11(a), the transmission phase response and amplitude response mostly varied along the vertical axis ($L_1$) at 14 GHz, and almost no change is observed along the horizontal axis ($L_2$). This means that $L_2$ has almost no influence on the transmission responses of the Ku band element. Similar cases are also observed for Fig. 11(b). The transmission performances varied only along the horizontal axis ($L_2$) at 20 GHz and did not change along the vertical axis ($L_1$). This indicates that the transmission responses of the K band elements are not affected by $L_1$. All the evidence demonstrate that the Ku and K band elements are well isolated from each other. Therefore, the phase compensation in the two bands can be calculated independently, thus greatly simplifying the design method.

## III. TRANSMITARRAY DESIGN AND MEASUREMENT

### A. DUAL-BAND TRANSMITARRAY DESIGN

Due to the high isolation between the two types of elements, the proposed dual-band TA is designed independently in each band. Given that the proposed dual-band TA has a large frequency span ranging from 14–20 GHz, it is difficult to cover such a wide frequency band using a single horn without degrading the performance. Therefore, two conical horns with −10 dB EI levels, which work in the Ku and K bands, are used to illuminate the proposed dual-band TA. The proposed dual-band TA has a circular aperture with diameters of 170 and 160 mm for the Ku and K bands, respectively.

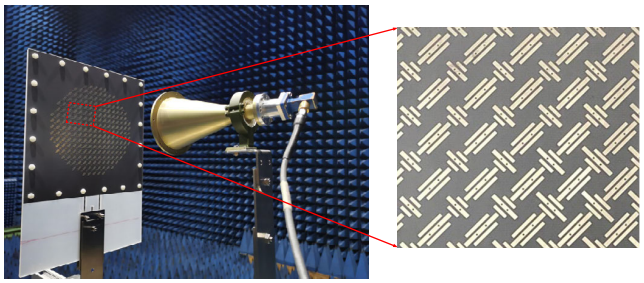

**FIGURE 12.** The measurement setup and the fabricated prototype of the proposed TA.

**TABLE 2.** Comparison of the proposed dual-band TA with previous designs.

| Ref. | N. of Lay. | N. of Sub. | Phase range | Band Ratio | Band-width (%) | Peak A. Eff. (%) |
|---|---|---|---|---|---|---|
| [21] | 4 | 0 | 360° | 1.5 | 3.3/3.4(3dB) | 52/53 |
| [22] | 3 | 2 | 0/180° | 1.5 | 10(3dB) | 20/21 |
| [23] | 3 | 0 | 300° | 1.14 | 6.8/5.4(1dB) | 38/34.6 |
| [24] | 3 | 3 | 300° | 1.14 | 7.2 /7.0(1dB) | 45/41.3 |
| [25] | 3 | 3 | 300° | 1.14 | 4.2 / 6.3(3dB) | 38/46 |
| **Pro.** | **2** | **1** | **360°** | **1.43** | **10/6 (1dB)** | **55/49** |

In both bands, $F/D$ is set at 1.37, which is determined by the equation: $\tan(\theta) = D/2F$, where $\theta$ is the half-illumination angle of the horn, and $D$ is the diameter of the TA ($\theta = 20°$, $D$ is 170 mm for the Ku band and 160 mm for the K band).

### B. SIMULATED AND MEASURED RESULTS

The designed dual-band TA is simulated by HFSS. To verify the reliability of the design method, the proposed TA has been designed, manufactured, and measured. The prototype of the proposed dual-band TA and the measurement setup are shown in Fig. 12. The fixtures and the slide rails are also designed and manufactured to obtain accurate measurement results. The proposed dual-band TA is measured in an anechoic chamber avoiding the influences of the measurement environment. Fig. 13 shows the simulated and measured radiation patterns of the proposed TA at 14 and 20 GHz. The simulated and measured gains versus frequency in both bands are shown in Fig. 14. The measurement results indicate that maximum gains of 25.2 and 27.4 dBi corresponding to aperture efficiencies of 55% and 49% are obtained at 13.75 and 20 GHz, respectively. A 1 dB bandwidth of 10% (12.9–14.35 GHz) and 6% (19.7–20.9 GHz) are also achieved in the Ku and K band, respectively. Small differences still remain in the tested and simulated results for the reasons of alignment errors of the feed horn, scattering effects of the metal fixing device and Printed Circuit Board manufacturing tolerances.

The comparisons between the proposed dual-band TA and previously published dual-band TAs are listed in Table 2. The proposed dual-band orthogonally polarized TA has better performance and simpler structure than previously published dual-band multi-layer stacked structures. The reasons are summarized as follows: high independence between the elements; good transmission amplitude in both bands; and the proposed elements are placed on the diagonal of the unit cell, which fully utilizes the space of the element and made it possible to obtain a 360° phase-shift range in both bands by using two types of orthogonal arrangement double-layer TA element. The proposed double-layer dual-band TA has a greatly simplified structure, an enhanced bandwidth, improved efficiency, and provides more possibilities for designing dual-band TA by using a double-layer structure.

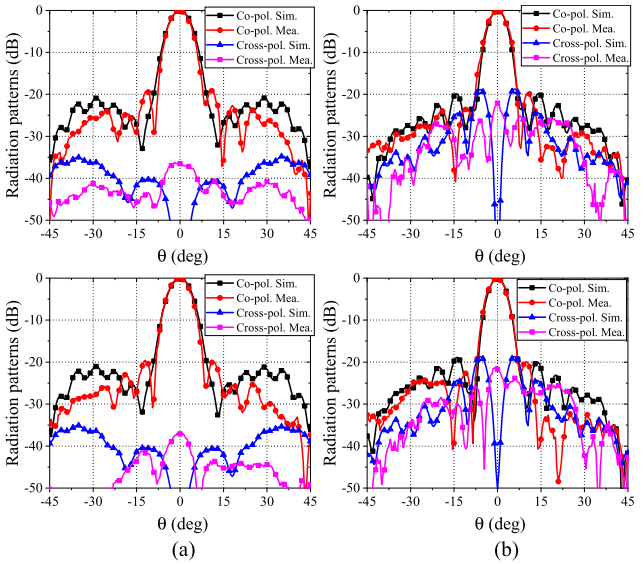


**FIGURE 13.** The simulated and measured normalized co-polar and cross-polar radiation patterns of the proposed TA. (a) 14 GHz, (b) 20 GHz ($\varphi = 0°$ plane at the left side and $\varphi = 90°$ at the right side).

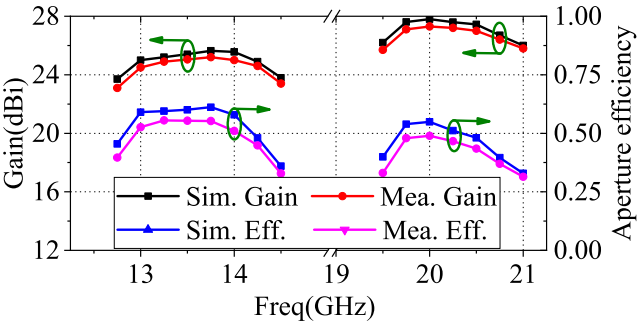


**FIGURE 14.** The simulated and measured gain versus frequency.

## IV. CONCLUSION

A double-layer dual-band orthogonally polarized highly efficient TA operated in the Ku/K bands (14 GHz/20 GHz) is presented for the SCS. Two types of multi-resonant dipoles with metal vias, separately operated in the Ku and K bands interlaced with each other independently in a circular aperture has been proposed for dual-band operation. A 360° phase shift range with transmission magnitude greater than −2 dB is achieved in the Ku and K bands independently. The proposed double-layer TA has been designed, manufactured,

and measured. The measurement results indicate that maximum gains of 25.2 and 27.4 dBi corresponding to aperture efficiencies of 55% and 49% are obtained at 13.75 and 20 GHz, respectively. In addition, the 1-dB gain bandwidths of 10% and 6% are also achieved in the Ku and K frequency bands, respectively. The proposed dual-band TA has good performance and paves the way for future base station arrays.

## REFERENCES

[1] D. Berry, R. Malech, and W. Kennedy, "The reflectarray antenna," *IEEE Trans. Antennas Propag.*, vol. AP-11, no. 6, pp. 645–651, Nov. 1963.
[2] D. M. Pozar, S. D. Targonski, and H. D. Syrigos, "Design of millimeter wave microstrip reflectarrays," *IEEE Trans. Antennas Propag.*, vol. 45, no. 2, pp. 287–296, Feb. 1997.
[3] J. A. Encinar, "Design of two-layer printed reflectarrays using patches of variable size," *IEEE Trans. Antennas Propag.*, vol. 49, no. 10, pp. 1403–1410, Oct. 2001.
[4] J. A. Encinar and J. A. Zornoza, "Broadband design of three-layer printed reflectarrays," *IEEE Trans. Antennas Propag.*, vol. 51, no. 7, pp. 1662–1664, Jul. 2003.
[5] H.-X. Xu, T. Cai, Y.-Q. Zhuang, Q. Peng, G.-M. Wang, and J.-G. Liang, "Dual-mode transmissive metasurface and its applications in multi-beam transmitarray," *IEEE Trans. Antennas Propag.*, vol. 65, no. 4, pp. 1797–1806, Apr. 2017.
[6] X. Zhong, L. Chen, Y. Shi, and X. Shi, "Design of multiple-polarization transmitarray antenna using rectangle ring slot elements," *IEEE Antennas Wireless Propag. Lett.*, vol. 15, pp. 1803–1806, 2016.
[7] C. Tian, Y.-C. Jiao, and G. Zhao, "Circularly polarized transmitarray antenna using low-profile dual-linearly polarized elements," *IEEE Antennas Wireless Propag. Lett.*, vol. 16, pp. 465–468, Jan. 2017.
[8] B. Rahmati and H. R. Hassani, "Low-profile slot transmitarray antenna," *IEEE Trans. Antennas Propag.*, vol. 63, no. 1, pp. 174–181, Jan. 2015.
[9] J. Yu, L. Chen, J. Yang, and X. Shi, "Design of a transmitarray using split diagonal cross elements with limited phase range," *IEEE Antennas Wireless Propag. Lett.*, vol. 15, pp. 1514–1517, 2016.
[10] S. H. Ramazannia Tuloti, P. Rezaei, and F. Tavakkol Hamedani, "High-efficient wideband transmitarray antenna," *IEEE Antennas Wireless Propag. Lett.*, vol. 17, no. 5, pp. 817–820, May 2018.
[11] Y. Chen, L. Chen, J.-F. Yu, and X.-W. Shi, "A C-band flat lens antenna with double-ring slot elements," *IEEE Antennas Wireless Propag. Lett.*, vol. 12, pp. 341–344, Mar. 2013.
[12] M. Euler and V. F. Fusco, "Frequency selective surface using nested split ring slot elements as a lens with mechanically reconfigurable beam steering capability," *IEEE Trans. Antennas Propag.*, vol. 58, no. 10, pp. 3417–3421, Oct. 2010.
[13] E. Erdil, K. Topalli, N. S. Esmaeilzad, O. Zorlu, H. Kulah, and O. A. Civi, "Reconfigurable nested ring-split ring transmitarray unit cell employing the element rotation method by microfluidics," *IEEE Trans. Antennas Propag.*, vol. 63, no. 3, pp. 1163–1167, Mar. 2015.
[14] A. H. Abdelrahman, A. Z. Elsherbeni, and F. Yang, "Transmission phase limit of multilayer frequency-selective surfaces for transmitarray designs," *IEEE Trans. Antennas Propag.*, vol. 62, no. 2, pp. 690–697, Feb. 2014.
[15] W. An, S. Xu, F. Yang, and M. Li, "A double-layer transmitarray antenna using Malta crosses with vias," *IEEE Trans. Antennas Propag.*, vol. 64, no. 3, pp. 1120–1125, Mar. 2016.
[16] X. Yi, T. Su, X. Li, B. Wu, and L. Yang, "A double-layer wideband transmitarray antenna using two degrees of freedom elements around 20 GHz," *IEEE Trans. Antennas Propag.*, vol. 67, no. 4, pp. 2798–2802, Apr. 2019.
[17] H.-H. Lv, Q.-L. Huang, X.-J. Yi, J.-Q. Hou, and X.-W. Shi, "Low-profile transmitting metasurface using single dielectric substrate for OAM generation," *IEEE Antennas Wireless Propag. Lett.*, vol. 19, no. 5, pp. 881–885, May 2020.
[18] X.-J. Yi, T. Su, B. Wu, J.-Z. Chen, L. Yang, and X. Li, "A double-layer highly efficient and wideband transmitarray antenna," *IEEE Access*, vol. 7, pp. 23285–23290, 2019.
[19] M. Cai, Z. Yan, X. Yi, S. Yang, and F. Fan, "An efficient method of generating vortex electromagnetic wave based on double-layer transmissive metasurface," *Int. J. RF Microw. Comput.-Aided Eng.*, vol. 30, no. 9, Sep. 2020, Art. no. e22325.
[20] M.-B. Cai, Z.-H. Yan, F.-F. Fan, S.-Y. Yang, and X. Li, "Double-layer 45° linearly polarized wideband and highly efficient transmitarray antenna," *IEEE Open J. Antennas Propag.*, vol. 2, pp. 104–109, 2021.
[21] R. Y. Wu, Y. B. Li, W. Wu, C. B. Shi, and T. J. Cui, "High-gain dual-band transmitarray," *IEEE Trans. Antennas Propag.*, vol. 65, no. 7, pp. 3481–3488, Jul. 2017.
[22] K. T. Pham, R. Sauleau, E. Fourn, F. Diaby, A. Clemente, and L. Dussopt, "Dual-band transmitarrays with dual-linear polarization at Ka-band," *IEEE Trans. Antennas Propag.*, vol. 65, no. 12, pp. 7009–7018, Dec. 2017.
[23] M. O. Bagheri, H. R. Hassani, and B. Rahmati, "Dual-band, dual-polarised metallic slot transmitarray antenna," *IET Microw., Antennas Propag.*, vol. 11, no. 3, pp. 402–409, Feb. 2017.
[24] A. Aziz, F. Yang, S. Xu, and M. Li, "An efficient dual-band orthogonally polarized transmitarray design using three-dipole elements," *IEEE Antennas Wireless Propag. Lett.*, vol. 17, no. 2, pp. 319–322, Feb. 2018.
[25] A. Aziz, F. Yang, S. Xu, M. Li, and H.-T. Chen, "A high-gain dual-band and dual-polarized transmitarray using novel loop elements," *IEEE Antennas Wireless Propag. Lett.*, vol. 18, no. 6, pp. 1213–1217, Jun. 2019.
[26] Y. Chen, W. Lin, S. Li, and A. Raza, "A broadband ±45° dual-polarized multidipole antenna fed by capacitive coupling," *IEEE Trans. Antennas Propag.*, vol. 66, no. 5, pp. 2644–2649, May 2018.
[27] Q. Wu, P. Liang, and X. Chen, "A broadband ±45° dual-polarized multiple-input multiple-output antenna for 5G base stations with extra decoupling elements," *J. Commun. Inf. Netw.*, vol. 3, no. 1, pp. 31–37, Mar. 2018.
[28] S.-H. Zhu, X.-S. Yang, J. Wang, N.-S. Nie, and B.-Z. Wang, "Mutual coupling reduction of ±45° dual-polarized closely spaced MIMO antenna by topology optimization," *IEEE Access*, vol. 8, pp. 29089–29098, 2020.
[29] W. Imbriale, S. Gao, and L. Boccia, Eds., *Space Antenna Handbook*. New York, NY, USA: Wiley, 2012.

**MINGBO CAI** was born in Xianyang, Shaanxi, China, in 1993. He received the B.S. degree in electronic and information engineering from Chang'an University, Xi'an, China, in 2011. He is currently pursuing the Ph.D. degree in electromagnetic field and microwave technology with Xidian University, Xi'an. His research interests include microstrip antenna arrays, reflector antenna, reflectarray antenna, and transmitarray antenna.

**ZEHONG YAN** was born in Tianmen, Hubei, China, in 1964. He received the B.S. and M.E. degrees in electromagnetic field and microwave technology from Xidian University, Xi'an, China, in 1980 and 1984, respectively, and the Ph.D. degree from Northwestern Polytechnical University, Xi'an, in 1996. In 1984, he joined Xidian University, where he is currently a Professor with the School of Electronic Engineering. His research interests include communications antenna, antenna tracking technology, and microwave device.

**FANGFANG FAN** (Member, IEEE) was born in Xianyang, Shaanxi, China. She received the B.S. degree from Xidian University, Xi'an, China, in 2003, the M.E. degree in electromagnetic field and microwave technology from the University of Electronic Science and Technology of China, in 2006, and the Ph.D. degree in electromagnetic field and microwave technology from Xidian University, in 2011. From March 2015 to March 2016, she went to the Chalmers University of Technology, Sweden, as a Visiting Scholar. Since 2006, she has been with Xidian University. She is currently an Associate Professor with the National Key Laboratory of Antennas and Microwave Technology, Xidian University. Her research interests include broadband and miniaturization antenna design, and gap waveguide technology and its application in antenna.

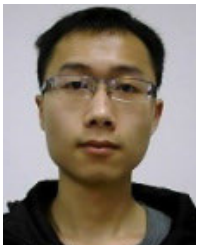

**SHUYANG YANG** was born in Baise, Guangxi, China, in 1993. He received the B.S. degree in electronic and information engineering from Xidian University, Xi'an, in 2016, where he is currently pursuing the Ph.D. degree. His research interests include reflector antennas, feed networks, reflectarray antenna, and transmitarray antenna.

**XI LI** was born in Weinan, Shaanxi, China, in 1991. He received the M.S. degree in electronic and information engineering from Xidian University, Xi'an, in 2019, where he is currently pursuing the Ph.D. degree. His research interests include microstrip array antenna, reflectarray antenna, and transmitarray antennas.